

## M2 Pore Mutations Convert the Glycine Receptor Channel from Being Anion- to Cation-Selective

Angelo Keramidas,\* Andrew J. Moorhouse,\* Chris R. French,\* Peter R. Schofield,<sup>†</sup> and Peter H. Barry\*

\*School of Physiology and Pharmacology, University of New South Wales, Sydney 2052, and <sup>†</sup>The Garvan Institute for Medical Research, Darlinghurst, Sydney 2010, Australia

**ABSTRACT** Three mutations in the M2 transmembrane domains of the chloride-conducting  $\alpha 1$  homomeric glycine receptor (P250 $\Delta$ , A251E, and T265V), which normally mediate fast inhibitory neurotransmission, produced a cation-selective channel with  $P_{Cl}/P_{Na} = 0.27$  (wild-type  $P_{Cl}/P_{Na} = 25$ ), a permeability sequence  $P_{Cs} > P_K > P_{Na} > P_{Li}$ , an impermeability to  $Ca^{2+}$ , and a reduced glycine sensitivity. Outside-out patch measurements indicated reversed and accentuated rectification with extremely low mean single channel conductances of 3 pS (inward current) and 11 pS (outward current). The three inverse mutations, to those analyzed in this study, have previously been shown to make the  $\alpha 7$  acetylcholine receptor channel anion-selective, indicating a common location for determinants of charge selectivity of inhibitory and excitatory ligand-gated ion channels.

### INTRODUCTION

The glycine receptor (GlyR) is a member of the ligand gated ion channel (LGIC) superfamily of neurotransmitter receptors, which mediate fast neurotransmission in the central nervous system. The other members of the LGIC family are the two subtypes of the  $\gamma$ -aminobutyric acid receptor (GABA<sub>A</sub>R, GABA<sub>C</sub>R), the nicotinic acetylcholine receptor (AChR), and a subtype of the 5-hydroxytryptamine receptors (5-HT<sub>3</sub>R). There is considerable structural homology among all members of the LGICs (Langosch et al., 1988) and intensive investigation has begun to shed some light on the various structural domains involved in the function of LGICs, although many questions concerning gating and permeation remain unresolved. These integral membrane protein receptors are all oligomeric, being composed of five subunits with each subunit having a large extracellular domain harboring the agonist/antagonist binding sites (Kuhse et al., 1995) and four transmembrane domains, designated M1 to M4, which form a central ion channel. Results from studies utilizing electron microscopy and a combination of site-directed mutagenesis and electrophysiology have confirmed earlier data, from experiments using labeled channel blockers, that the M2 transmembrane domains contribute to the lining of the channel pore (see Fig. 1 and Karlin and Akabas, 1995). Binding of neurotransmitter to residues in the extracellular domains is believed to cause lateral twisting of the M2 domains, resulting in an enlargement of the channel pore as the receptor-channels convert from their closed, non-conducting conformation to

an open, conducting one (Sansom, 1995; Unwin, 1995; Lynch et al., 1997). Detailed evidence now exists that the AChR channel (Wilson and Karlin, 1998) and the GABA<sub>A</sub>R channel (Xu and Akabas, 1996) are narrowest at the intracellular end, where the greatest interactions with permeating ions may be expected. Electrophysiology and site-directed cysteine mutagenesis, using the substituted cysteine accessibility method (SCAM), have determined that as a result of conformational rearrangement of the M2 domains, different residues are exposed to the pore lumen between the closed and open states in both the GABA<sub>A</sub>R (Xu et al., 1995; Xu and Akabas, 1996) and the AChR (Pascual and Karlin, 1998; Wilson and Karlin, 1998).

Crucial to the role of LGICs in brain function is the nature of the permeating ions. Despite the close sequence and structural homology found between LGIC M2 domains, the fundamental question remains: "How is ion selectivity and anion/cation discrimination achieved?" Homomeric AChRs, which are cation-selective, have negatively charged rings composed of either glutamate residues (extracellular ring) or aspartate residues (cytoplasmic ring) and an additional intermediate negatively charged ring close to the intracellular mouth of the pore (Imoto et al., 1988; see Fig. 1). In addition, AChRs have a central ring of polar residues, three residues extracellular to the intermediate ring (Imoto et al., 1991). The 5-HT<sub>3</sub>R has a similar arrangement of three negatively charged rings and a central polar ring. In contrast, the GlyR and GABA<sub>A</sub>R, which are anion-selective, have two positively charged rings composed of arginine residues at the intra- and extra-cellular mouths of the ion pore (Fig. 1). Mutation studies have proved these charged rings to be important determinants of channel conductance for monovalent cations in AChRs, with the magnitude of the conductance linearly decreasing with the magnitude of net negative charge, the decrease being greatest for changes for the intermediate ring (Imoto et al., 1988, 1991; Konno et al., 1991; Wang and Imoto, 1992). In  $\alpha 1$  homomeric GlyRs, mutations to the positively charged extracellular ring have

Received for publication 27 December 1999 and in final form 17 March 2000.

Address reprint requests to Prof. Peter H. Barry, School of Physiology and Pharmacology, University of New South Wales, Sydney 2052, Australia. Tel.: +61-2-9385-1101; Fax: +61-2-9385-1099; E-mail: p.barry@unsw.edu.au.

© 2000 by the Biophysical Society  
0006-3495/00/07/247/13 \$2.00

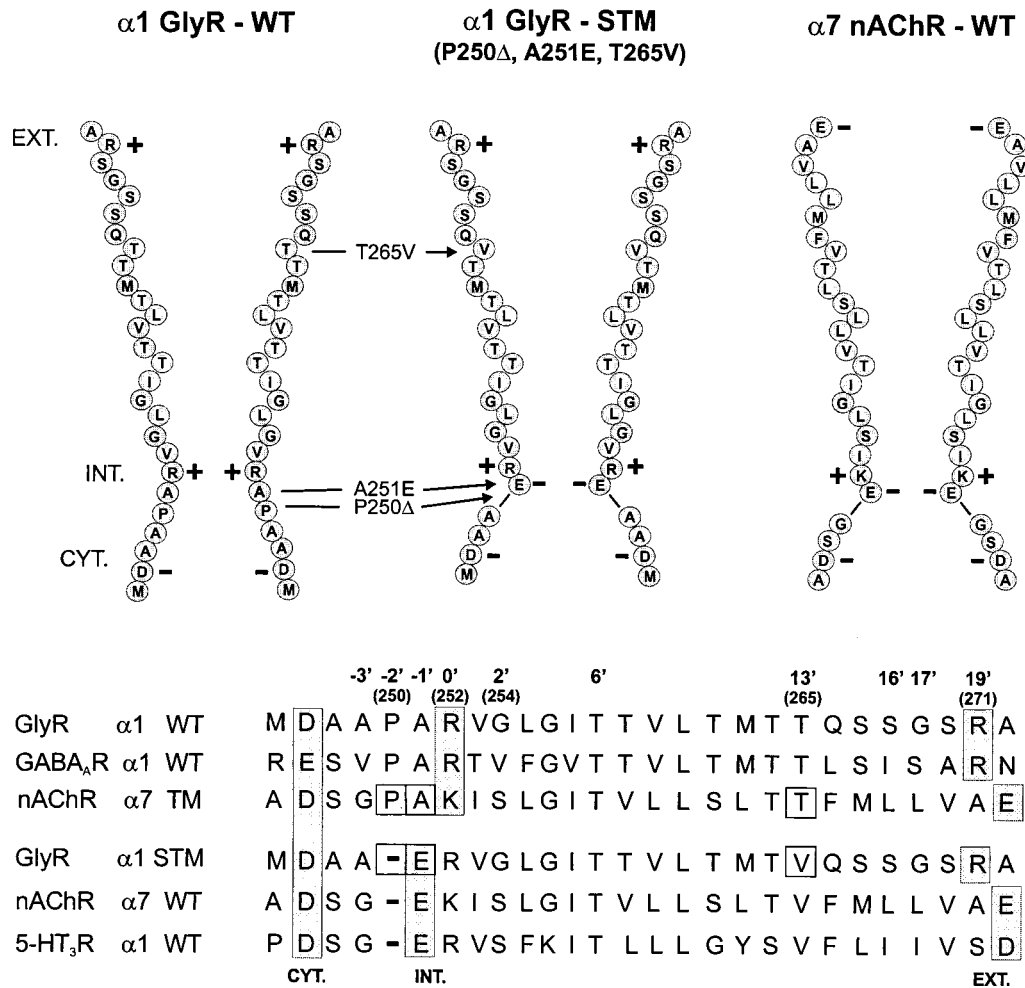


FIGURE 1 A schematic representation of two M2 transmembrane domains and the corresponding pore profiles of homomeric wild-type (WT) and selectivity triple mutant (STM)  $\alpha 1$  glycine receptor channels (GlyRs), together with a WT  $\alpha 7$  neuronal nicotinic acetylcholine receptor channel (nAChR) for comparison. Amino acids are shown as circles with their single-letter code and, where it applies, their charge is indicated adjacent to the residues. Arrows mark the STM mutations. The top three rows list selected M2 domain amino acid sequences for anion-selective channels: WT  $\alpha 1$  GlyR,  $\alpha 1$  GABA<sub>A</sub>R, and the triple mutant  $\alpha 7$  nAChR (TM; Galzi et al., 1992; Corringer et al., 1999); the bottom three rows list cation-selective channels: STM GlyR, WT  $\alpha 7$  nAChR, and WT  $\alpha 1$  5-HT<sub>3</sub>R for comparison. The STM mutations in this study and the TM ones of Galzi et al. (1992) are boxed. The cytoplasmic (CYT.), intermediate (INT.), and extracellular (EXT.) rings of charge (Imoto et al., 1988) are shown in the schematic and the corresponding sequences. They are also boxed and shaded. The numbering of the GlyR  $\alpha 1$  subunit is indicated above the sequence in parentheses. To assist comparison among the M2 domains of different LGIC members we also include a universal LGIC numbering system based on Miller (1989), where the intermediate positively charged R or K in the M2 domains are designated as 0'.

also demonstrated comparable decreases in channel conductance when the charge was replaced by neutral residues (Langosch et al., 1994; Rajendra et al., 1995). In none of the above studies, however, was there any reported change in cation/anion selectivity.

The first example of charge selectivity conversion in an ion channel was provided by Galzi et al. (1992), who used a systematic mutagenesis approach in recombinant  $\alpha 7$  nAChR homomers to address the issue of charge discrimination in LGICs. Seven of the residues in the M2 region of the  $\alpha 7$  nAChR, which were considered to be important for permeation, were replaced by the equivalent residues of the

$\alpha 1$  GlyR, and the mutated nAChR ion channel became anion-selective. The minimum number of residues required to alter the selectivity of the cationic AChR to anionic was three: a proline insertion at position -2' (P-2'; refer to Fig. 1 and legend for universal LGIC residue numbering nomenclature relative to the intermediate positive R or K residue) near the intracellular border of M2, mutation of the adjacent glutamate (E-1'A), and a more central mutation (V13'T). Subsequent studies by Corringer et al. (1999) verified the inference that the proline insertion was a critical component for the selectivity conversion via a conformational or geometrical change to the constricted region of the pore. A

concomitant conclusion was that the constricted region contributes to the selectivity filter of the channel.

Little, however, is known about the structural determinants of selectivity in the anion-selective LGICs and how conserved these selectivity determinants are across the LGIC superfamily. Therefore, we have investigated whether the analogous inverse set of triple mutations to those done in the nAChR changes the charge selectivity of the GlyR channel from anionic to cationic, as found in the AChR, and, if so, whether the subsequent results give us any further information about the molecular mechanisms underlying selectivity. We will henceforth refer to our set of GlyR mutations as the selectivity triple mutation, or STM.

## MATERIALS AND METHODS

### Transient expression of recombinant $\alpha 1$ subunit GlyRs in HEK293 cells

The complementary DNA (cDNA) encoding the wild type (WT) or mutant  $\alpha 1$  subunit of the human GlyR was subcloned into the pCIS expression vector. Site-directed point mutations in the cDNA were constructed using the oligonucleotide-directed polymerase chain reaction (PCR) mutagenesis method and confirmed by sequencing the cDNA clones. Plasmid DNA encoding WT or mutant  $\alpha 1$  subunits of the human GlyR were transfected into exponentially growing HEK293 cells using the calcium phosphate precipitation method of Chen and Okayama (1987). In addition, the cells were transfected with a separate plasmid containing the cDNA for the CD4 surface antigen. This enabled transfected cells to express surface antigens so that they could be coated with CD4 antibody-coated polystyrene beads (Dynabeads M-450, CD-4; Dynal, Great Neck, NY). The GlyR mutations used were the three equivalent inverse mutations in the M2 region to those used in the AChR triple mutation by Galzi et al. (1992). These were the deletion of the cytoplasmic proline (P250 $\Delta$ ; P-2' $\Delta$ ), the mutation of the adjacent alanine to a glutamate (A251E; A-1'E) and the mutation of a threonine to a valine (T265V; T13'V), as indicated in Fig. 1.

### Solutions

In all the experiments the standard intracellular (pipette) solution consisted of (all solute concentrations in mM): 145 NaCl, 2 CaCl<sub>2</sub>, 2 MgCl<sub>2</sub>, 10 HEPES, and 5 EGTA adjusted to pH 7.3 with NaOH. The control extracellular solution consisted of 145 NaCl, 2 CaCl<sub>2</sub>, 2 MgCl<sub>2</sub>, 10 HEPES, and 10 glucose. For the dilution potential experiments (both WT and STM GlyRs) the 145 mM NaCl was replaced with 75 mM NaCl and 136 sucrose (50% dilution) or 37.5 mM NaCl and 189 sucrose (25% dilution). Sucrose was added to maintain isoosmolar conditions. Each solution was adjusted to pH 7.4 with NaOH. For the STM GlyR Na<sup>+</sup> versus test cation solutions, the 145 mM NaCl in the control extracellular solution (above) was replaced by one of the following (in mM): 145 CsCl, 145 KCl, 145 LiCl or 50 CaCl<sub>2</sub> with 53 NaCl. The CsCl and KCl solutions were adjusted to pH 7.4 with CsOH or KOH, respectively, while the LiCl and CaCl<sub>2</sub>/NaCl solutions were adjusted to pH 7.4 with NaOH. For the precise ionic concentrations refer to the appropriate figure legends. All solutions were kept refrigerated and discarded after one to two weeks. Glycine was dissolved into the appropriate extracellular solution to give final concentrations, as indicated in the text.

Application of solutions to the recorded cell was achieved using a gravity-fed parallel array of polythene microperfusion tubes, fixed adjacent to each other with slow-setting epoxy resin (Araldite, Selleys, Aust.) and mounted on an electromechanical micromanipulator. For single channel experiments, a bath perfusion system was used.

## Electrophysiology

Experiments were performed at a room temperature of 20°C. All patch pipettes were pulled using a two-stage electrode puller (P-87, Sutter Instruments, Novato, CA) and fire-polished. The patch pipette was secured to a holder and connected to an Ag/AgCl wire and mounted on a 3-axis hydraulic micromanipulator (Narishige Scientific Instrument Lab, Tokyo, Japan) for whole-cell experiments, or a 3-axis piezoelectric micromanipulator (Burleigh Instruments Inc., Fishers, NY) for outside-out patch experiments. Liquid junction potentials arising from pipette and bath solutions were calculated using the MS Windows version of the software package JPCalc (Barry, 1994: contact PHB for program availability) and accounted for, when setting membrane voltages during each experiment. All experiments were performed in voltage-clamp mode. Off-line analysis and graphing were conducted using pCLAMP 6.0.4 (Axon Instruments, Foster City, CA) or SigmaPlot (Jandel Scientific, San Rafael, CA). All data are expressed as mean  $\pm$  SEM.

### Whole-cell current-voltage (*I-V*) recordings

Whole-cell membrane currents were recorded using an Axopatch-1D amplifier, digitized using a Digidata 1200 A/D board and recorded using pCLAMP 6.0.4 software (all from Axon Instruments) on a Pentium 166 MHz computer. Currents were filtered, with the 4-pole Bessel filter provided on the amplifier, at 200 or 500 Hz ( $-3$  dB) and acquired at a sampling frequency of 1 kHz. Patch pipettes were made using borosilicate hematocrit tubes (Vitrex-1601, Herlev, Denmark). Their resistances, when filled with intracellular solution and measured in the bath solution, ranged between 1.1 and 2.7 M $\Omega$ . Whole-cell seal resistances ranged between 1 and 5 G $\Omega$  before whole-cell configurations were established. Series resistances ranged between 2 and 11 M $\Omega$  and were compensated by between 65–80%. Due to the large whole-cell WT currents, the WT experiments were compensated for at the lower end of this range. The *I-V* experiments were performed by holding the cell membrane at potentials (in mV) of  $-60$ ,  $-30$ ,  $-15$ ,  $0$ ,  $+15$ ,  $+30$ , and  $+60$ , and recording glycine-activated currents at each membrane potential. Whole-cell currents were recorded from the above membrane voltages in one extracellular solution before switching to another extracellular solution (e.g., NaCl dilution or test cation). In nearly all cases, experimental runs across the entire voltage range were repeated to check for consistency in reversal potential. Peak whole-cell currents were measured for each corresponding membrane voltage and fitted to a quadratic polynomial, generally between  $-30$  mV and  $+30$  mV. Bath application of glycine lasted for  $\sim 4$ – $5$  s. Patch electrodes were tested at the end of each experiment for any voltage drift, which was accounted for if the magnitude exceeded 1 mV. In most cases, the amount of drift was minimal and no correction was required. Reversal potential ( $V_{rev}$ ) values were read directly from the finalized *I-V* plots for each cell and averaged. To determine anion-cation permeability ratios, data points averaged from cells, where all three extracellular NaCl concentrations were used, were plotted and then fitted to the Goldman-Hodgkin-Katz (GHK) equation. In order to compensate for any slight offsets in cell composition and the whole-cell recording system we used shifts in  $V_{rev}$  measured in symmetrical conditions (where  $V_{rev}$  should be close to zero) before plotting and fitting the corrected data to the GHK equation:

$$V_{rev} = \left( \frac{RT}{F} \right) \ln \left\{ \frac{P_{Na}(a_{Na})_o + P_{Cl}(a_{Cl})_i}{P_{Na}(a_{Na})_i + P_{Cl}(a_{Cl})_o} \right\} \quad (1)$$

Where  $V_{rev}$  is the potential at which the current is zero,  $R$  is the gas constant,  $T$  is temperature in Kelvin,  $F$  is Faraday's constant,  $P_{ion}$  is the permeability of the ion, and  $(a_{ion})$  is the activity of the ion in the extracellular (subscript o) or intracellular (subscript i) solutions. To eliminate the dependence on  $[Na^+]_i$  and the small variability in  $V_{rev}$  values in "symmetrical" (or control) conditions (see averaged value in Fig. 5), a

modified form of the GHK equation was derived for determining the relative alkali cation permeability ratios,  $P_X/P_{Na}$ :

$$\Delta V_{rev} = V_{rev}^T - V_{rev}^C$$

$$= \left( \frac{RT}{F} \right) \ln \left[ \frac{(a_{Na})_o^T + P_X/P_{Na}(a_X)_o + P_{Cl}/P_{Na}(a_{Cl})_i}{(a_{Na})_o^C + P_{Cl}/P_{Na}(a_{Cl})_i} \right] \quad (2)$$

Where the superscripts T and C denote test cation solution and "symmetrical" (control) solutions, respectively, and the  $[(a_{Na})_i + P_{Cl}/P_{Na}(a_{Cl})_o]$  term for both solutions will essentially cancel out. X represents the test monovalent cation.

The  $P_{Ca}/P_{Na}$  ratio was also calculated using the generalized version of the current-voltage equation at zero current (e.g., Barry and Gage, 1984):

$$\sum_j I_j = \sum_j \left\{ P_j z_j^2 V_{rev} \frac{F^2 [a_j^o - a_j^i \exp(z_j V_{rev} F/RT)]}{RT [1 - \exp(z_j V_{rev} F/RT)]} \right\}$$

$$= 0 \quad (3)$$

Where  $P_j$  and  $z_j$  are the permeability and valency of ion j, respectively,  $I_j$  is the current, and superscripts o and i denote extracellular and intracellular solutions, respectively. Ion activities were determined directly from tabulated data of Robinson and Stokes (1965) or, where necessary, interpolated from such values using graphical and computational procedures.

### Single channel recordings

Single channel currents were recorded from excised outside-out membrane patches, held at membrane potentials of +60 mV and -60 mV, in response to bath application of glycine. Patch pipettes were made using thick-walled borosilicate tubes (GC150F-15, Clark Electromedical Instruments, Reading, UK), coated with Sylgard (Dow Corning, Midland, MI) and had final resistances of 7–14 M $\Omega$  when filled with pipette solution. In both the pipette and bath solution  $Na^+$  and  $Cl^-$  were the only monovalent ions present (149.8 mM  $Na^+$ , 153 mM  $Cl^-$ ). Currents were recorded with pCLAMP 6.0.4 software and an Axopatch 200B amplifier (Axon Instruments), and were digitized directly at 10 kHz onto the hard disk of a 166 MHz Pentium computer (via a Digidata 1200 A/D board, Axon Instruments) after filtering at 2 kHz with the amplifier's 4-pole Bessel filter. Single channel conductances, for WT GlyRs, were calculated by fitting Gaussian distributions to all point amplitude histograms, the peaks of which were confirmed by direct measurements. In addition, a stationary noise analysis was conducted on current records from both WT and STM GlyRs (e.g., Gray, 1994). For this analysis, the mean current and the variance around this mean were measured from 30 to 60 s of continuous current recordings taken before, during, and after glycine application. Values from the periods flanking glycine application were averaged, and this average was subtracted from values obtained during glycine application. Unitary current amplitude was then obtained from the glycine-induced change in variance divided by the glycine-induced change in mean current. This simplified relationship assumed a low probability of GlyR channel opening and was justified by the fact that the conductance values obtained from noise analysis at different glycine concentrations were similar, with an approximately linear relationship between mean current and variance. The assumption was further reinforced for the WT GlyRs by the agreement between noise analysis and the contribution of the directly measured major conductance levels (see Results) and for the STM GlyRs by the very flickery and brief nature of the current fluctuations. Conductances were calculated by dividing the unitary current by the driving force (with the channel reversal potential assumed to be close to 0 mV in symmetrical control solutions).

## RESULTS

### Expression and general current properties of STM $\alpha 1$ subunit GlyRs

Transient transfection of the STM (P250 $\Delta$ , A251E, and T265V)  $\alpha 1$  GlyR subunit into HEK293 cells showed low levels of glycine-activated currents, which were only observable 1) in cells that were heavily labeled with the transfection marker CD4 antibody beads (thus implying much greater levels of STM GlyR expression than average), and 2) in the presence of higher concentrations of glycine (e.g., 50 mM and 100 mM). Under these conditions, small but clearly discernible glycine-activated whole-cell currents (e.g., see Fig. 3) and a glycine-activated increase in noise in outside-out patch recordings (e.g., Fig. 7) were observed. The lack of any current responses for cells with low GlyR expression served as a control for any osmotically activated currents.

Both whole-cell and single channel glycine-activated currents were substantially reduced (generally by two orders of magnitude) compared to those of WT GlyRs (e.g., see Figs. 2 and 6, respectively) and only cells passing whole-cell currents >100 pA at a membrane potential of -60 mV were accepted for analysis. A 100 mM glycine concentration was used to elicit whole-cell currents for the STM GlyRs, and 1, 25, and 100 mM glycine for single channel currents. In contrast, a supramaximal agonist concentration of 1 mM was used for WT whole-cell currents ( $EC_{50} \sim 30 \mu M$ ; Rajendra et al., 1994; see also Bormann et al., 1993) and 1–100  $\mu M$  for single channel currents. The high agonist concentrations needed for current elicitation in the STM GlyRs suggest an increase in the  $EC_{50}$  for the mutant receptors. Interestingly, the equivalent anion-selective triple mutation in the neuronal  $\alpha 7$  nAChR showed a decrease in the  $EC_{50}$  (Galzi et al., 1992).

### Dilution potential experiments for WT and STM GlyRs: anionic-to-cationic conversion

Extracellular NaCl dilutions were used to verify and ascertain the selectivity properties of WT and STM GlyRs, respectively. In all cases  $[Cl^-]_i = 153$  mM and  $[Na^+]_i = 162.9$  mM. As illustrated in Fig. 2,  $I$ - $V$  curves of WT whole-cell currents showed that the average reversal potential ( $V_{rev}$ ) shifted in the positive direction as  $[NaCl]_o$  was progressively reduced for the same cell, from an approximately symmetrical NaCl (153 mM  $Cl^-$ ) to a dilution of NaCl to 50% (83 mM  $Cl^-$ ), and finally to a dilution of NaCl to 25% (45.5 mM  $Cl^-$ ). This clearly confirmed that WT  $\alpha 1$  GlyRs are predominantly  $Cl^-$ -selective, with the reversal potential tending toward the values of  $E_{Cl}$ , as predicted by the Nernst equation for chloride.

The prominent rapid decays in current traces of the WT GlyRs seemed to be very much greater for cells with typi-

cally large current magnitudes, suggesting that this is more likely to be caused by concentration polarization effects ( $\text{Cl}^-$  shift) rather than by actual receptor desensitization. In contrast, the STM GlyRs did not show such prominent current decays, presumably because these currents were relatively small and any concentration polarization effects would be minimal. The experimental values of  $V_{\text{rev}}$  ( $-2.9$  mV) agreed well with the predicted value ( $-2.0$  mV).

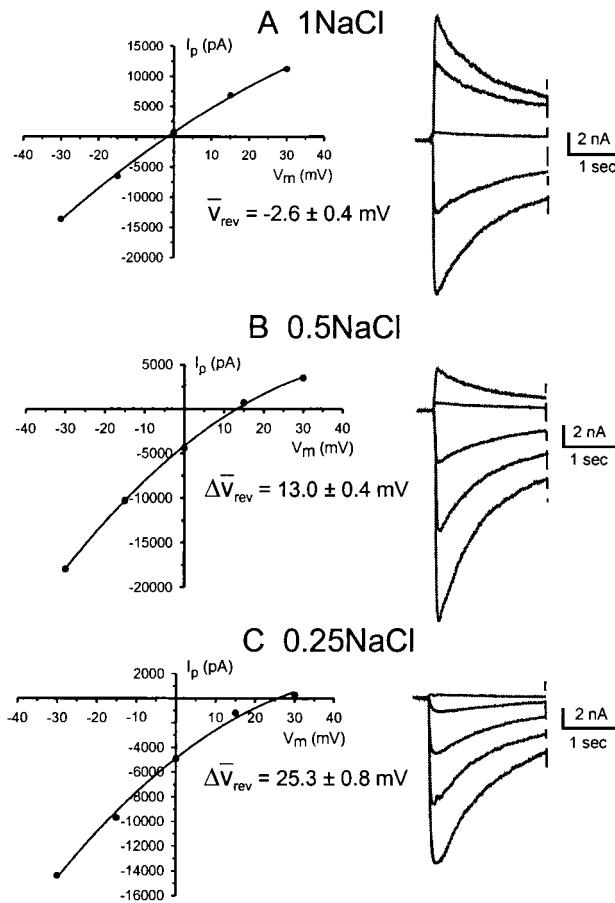


FIGURE 2 Sample dilution potential experiment for WT  $\alpha 1$  homomeric GlyRs. Whole-cell glycine activated current responses recorded from the same cell (right panels) in the presence of different extracellular NaCl concentrations. The dilution ratios relative to the intracellular (pipette) concentration are  $\sim 1$  for (A) 1 NaCl, 0.5 for (B) 0.5 NaCl, and 0.25 for (C) 0.25 NaCl. Corresponding peak whole-cell current ( $I_p$ ) was plotted against membrane voltage ( $V_m$ ) to generate the current-voltage ( $I$ - $V$ ) plots (left panels); plotted between a membrane potential range of  $-30$  mV to  $+30$  mV and fitted to a quadratic polynomial). The plots show a positive shift in reversal potential, toward  $E_{\text{Cl}}$ , as extracellular  $[\text{NaCl}]$  is reduced. (A) Symmetrical  $\text{Cl}^-$  (153 mM), (B)  $[\text{Cl}^-]_i = 153$  mM,  $[\text{Cl}^-]_o = 83$  mM, and (C)  $[\text{Cl}^-]_i = 153$  mM,  $[\text{Cl}^-]_o = 45.5$  mM.  $\text{Na}^+$  concentrations approximate  $\text{Cl}^-$  values. The averaged reversal potential ( $V_{\text{rev}}$ ) in control and shifts in reversal potential ( $\Delta V_{\text{rev}}$ ) for dilutions are shown for  $n = 8$  experiments. For presentation purposes, the current traces have had additional off-line filtering (100 Hz), data reduction ( $\times 2$ ), and their durations have been truncated.

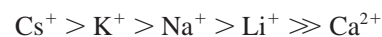
The same experimental procedure was used for cells expressing the STM GlyRs. Fig. 3 represents an example of a typical experiment done on one cell, with the averaged  $V_{\text{rev}}$  and  $\Delta V_{\text{rev}}$  values included for all cells in Fig. 3. With progressive decreases in  $[\text{NaCl}]_o$ , from an approximately symmetrical NaCl concentration to dilutions to 50% and 25%, the reversal potential shifted in the negative direction. This is consistent with the STM GlyRs being cation-selective channels, with  $V_{\text{rev}}$  tending toward values for  $E_{\text{Na}}$ , as predicted by the Nernst equation for  $\text{Na}^+$ . There were no other monovalent cations present on either side of the cell membrane.

### Anion-to-cation permeability ratios for WT and STM GlyRs

The corrected  $V_{\text{rev}}$  values obtained in the above dilution potential experiments for WT and STM were plotted against activity of extracellular  $\text{Cl}^-$  or  $\text{Na}^+$ , respectively, as illustrated in Fig. 4. Fitting these data points to the Goldman-Hodgkin-Katz (GHK) equation revealed the permeability ratio,  $P_{\text{Cl}}/P_{\text{Na}}$  for WT as  $24.6 \pm 0.7$  ( $n = 8$ , Fig. 4 A), and  $0.27 \pm 0.01$  for STM GlyRs ( $n = 4$ , Fig. 4 B; see also Table 1). Again, these values clearly demonstrated that the STM has converted the GlyR from an anion-selective channel into a cation-selective one, with a considerable change in selectivity.

### Cation permeability ratios for STM GlyRs

The results of the dilution potential experiments, mutating three residues in the STM GlyRs, imparted relatively radical changes in the anion:cation selectivity properties of these GlyRs. To further investigate the properties of permeation through the STM GlyR channels,  $I$ - $V$  experiments under essentially bi-ionic conditions were performed on the STM GlyRs to determine their relative cation permeability. Sample  $I$ - $V$  plots for a range of cations are provided in Fig. 5. Each panel in the figure consists of a pair of  $I$ - $V$  curves obtained from the same cell, where the extracellular solution was replaced from one containing approximately symmetrical  $\text{Na}^+$  concentrations (left curves) to one containing a test cation in the external solution ( $X$ , right curves). Therefore, the test cations whose reversal potential shifted in a positive direction (compared to the symmetrical NaCl values), represent cations more permeant than  $\text{Na}^+$ , while those whose reversal potential shifted in a negative direction correspond to cations less permeant than  $\text{Na}^+$ . These results revealed that the STM GlyR has a cation permeability sequence of:



For the monovalent cations, this represents a low-field-strength sequence (Eisenman sequence I or II; Eisenman

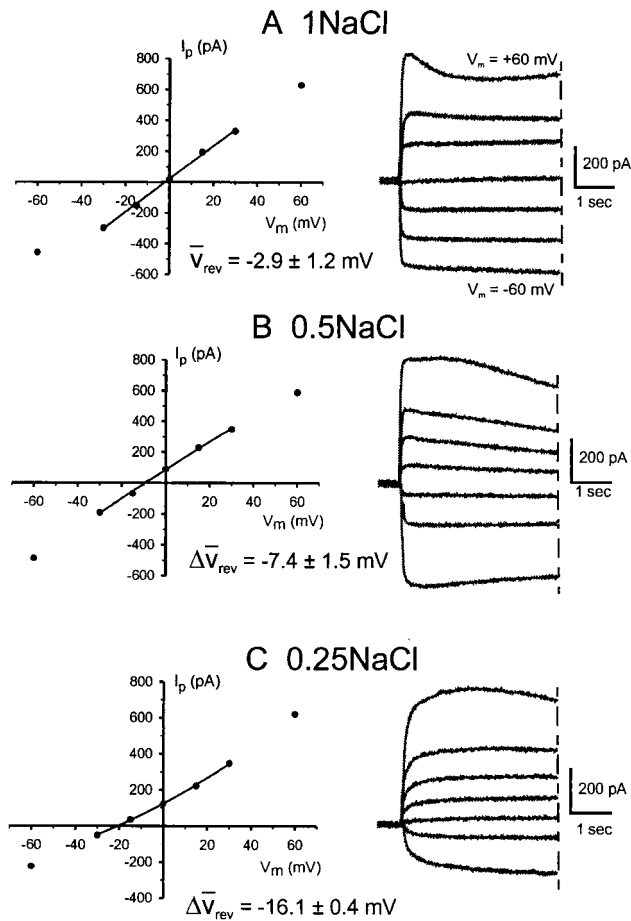


**FIGURE 3** Sample dilution potential experiment for selectivity triple mutant (STM)  $\alpha 1$  homomeric GlyRs. Whole-cell glycine-activated current responses recorded from the same cell (*right panels*) in the presence of different extracellular NaCl concentration dilutions. The dilution ratios relative to the intracellular (pipette) concentration are  $\sim 1$  for (A) 1 NaCl, 0.5 for (B) 0.5 NaCl, and 0.25 for (C) 0.25 NaCl. Corresponding peak whole-cell current ( $I_p$ ) was plotted against membrane voltage ( $V_m$ ) to generate the  $I$ - $V$  plots (*left panels*; plotted between a membrane potential range of  $-60$  mV to  $+60$  mV and fitted to a quadratic polynomial between  $-30$  mV and  $+30$  mV, which produced a more accurate determination of  $V_{rev}$ ). The plots show a negative shift in reversal potential, toward  $E_{Na^+}$ , as the extracellular  $[NaCl]$  is reduced. In all cases,  $[Na^+]_i = 162.9$  mM and (A)  $[Na^+]_o = 149.8$  mM, (B)  $[Na^+]_o = 79.7$  mM, and (C)  $[Na^+]_o = 42.2$  mM.  $Cl^-$  concentrations approximate  $Na^+$  values. The averaged reversal potential ( $V_{rev}$ ) in control and shifts in reversal potential ( $\Delta V_{rev}$ ) for dilutions are shown for  $n = 4$  experiments. For presentation purposes (as in Fig. 2), the current traces have had additional off-line filtering (100 Hz), data reduction ( $\times 2$ ), and their durations have been truncated.

and Horn, 1983), suggesting only weak interactions of the ion with binding sites within the pore during permeation. In fact, the relative cation permeability sequence corresponds to the relative mobility sequence of these cations in free solution (Robinson and Stokes, 1965; see also Barry and Gage, 1984; Barry and Lynch, 1991). That is, the cations pass through the STM channels in order of hydrated ion radius, with  $Cs^+$  being the smallest, followed by  $K^+$ ,  $Na^+$ ,

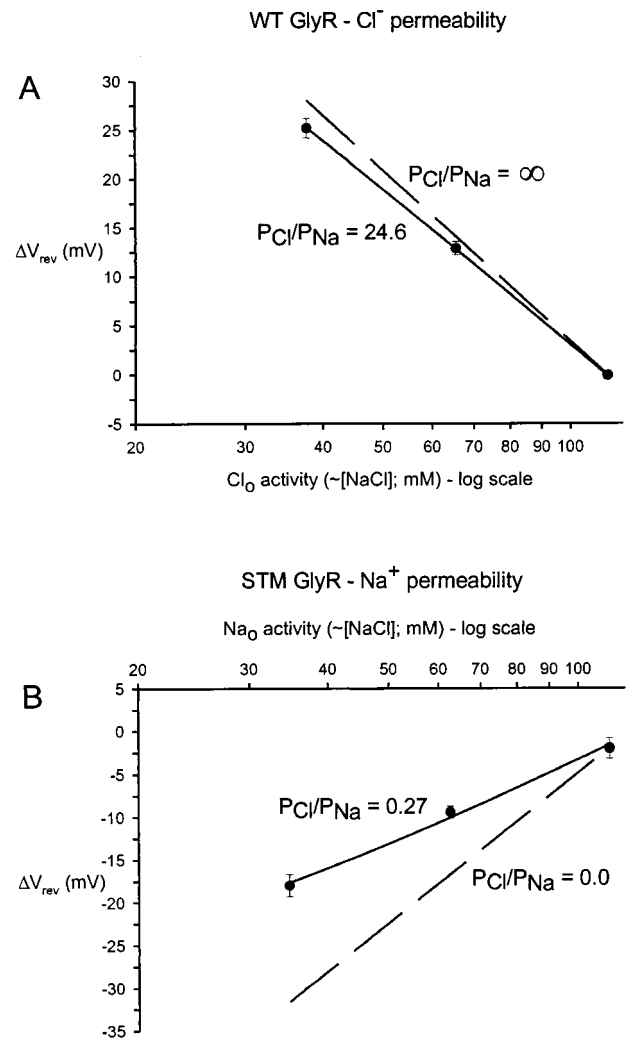


**FIGURE 4** Reversal potential-activity plots for determining relative anion-cation permeability ratios through WT and STM homomeric  $\alpha 1$  GlyR channels. (A) The corrected reversal potential shift ( $\Delta V_{rev}$ ) is plotted against extracellular  $Cl^-$  activity ( $a_{Cl^-}$ ) for WT GlyRs. For permeability fitting, the shift in reversal potential was used to allow for a small  $-2.5$  mV shift from a predicted  $-0.1$  mV offset present in WT symmetrical NaCl data (see Figs. 2 and 3 and Materials and Methods). The fitted value of  $P_{Cl^-}/P_{Na^+} = 24.6$  ( $P_{Na^+}/P_{Cl^-} = 0.041$ ). (B) The corrected reversal potential shift ( $\Delta V_{rev}$ ) is plotted against extracellular  $Na^+$  activity ( $a_{Na^+}$ ) for STM GlyRs, ( $P_{Cl^-}/P_{Na^+} = 0.27$ ). The data points were fitted to the Goldman-Hodgkin-Katz equation (*solid lines*), using ion activities;  $\Delta V_{rev} = RT/F \ln\{[P_{Na^+}(a_{Na^+})_o + P_{Cl^-}(a_{Cl^-})_i]/[P_{Na^+}(a_{Na^+})_i + P_{Cl^-}(a_{Cl^-})_o]\}$  to determine  $P_{Cl^-}/P_{Na^+}$ . The dashed line in each case represents the hypothetical situation, where  $P_{Na^+}$  or  $P_{Cl^-} = 0$ , as given by the appropriate equilibrium potentials ( $E_{Cl^-}$  or  $E_{Na^+}$ ) as a function of extracellular ion activity.

and  $Li^+$ . Using the averaged  $\Delta V_{rev}$  values (Fig. 5) obtained for these experiments and the ratio  $P_{Cl^-}/P_{Na^+}$  already determined in the dilution potential experiments, the permeability ratio  $P_X/P_{Na^+}$  was quantified with the Goldman-Hodgkin-Katz equation (Eq. 2). The calculated permeability ratios in order of decreasing permeability for monovalent cations were  $P_{Cs^+}/P_{Na^+} = 1.76 \pm 0.07$  ( $n = 5$ ),  $P_{K^+}/P_{Na^+} = 1.53 \pm 0.02$

**TABLE 1** Anion-to-cation permeability ratios for WT and STM GlyRs obtained from reversal potential experiments (see Figs. 2 and 3) and cation-to-cation permeability ratios for STM GlyRs obtained from bi-ionic potential experiments (see Fig. 5). Values are given as mean  $\pm$  SEM

Permeability ratio relative to $P_{\text{Na}}$	$n$	WT	STM
$P_{\text{Cl}}$	8	$24.6 \pm 0.7$	$0.27 \pm 0.01$
$P_{\text{Cs}}$	4	—	$1.76 \pm 0.07$
$P_{\text{K}}$	5	—	$1.53 \pm 0.02$
$P_{\text{Li}}$	4	—	$0.72 \pm 0.01$
$P_{\text{Ca}}$	4	—	$\approx 0$

( $n = 4$ ), and  $P_{\text{Li}}/P_{\text{Na}} = 0.72 \pm 0.01$  ( $n = 4$ ; Table 1). Hence, the STM channels poorly discriminate between monovalent cations, as also found for the native AChR channel (e.g., Adams et al., 1980; Barry and Gage, 1984).

### Divalent cation permeability in STM GlyRs

Since the neuronal  $\alpha 7$  nAChR is highly permeable to  $\text{Ca}^{2+}$  ( $P_{\text{Ca}}/P_{\text{Na}} \sim 10$ , Bertrand et al., 1993), we investigated the permeability of  $\text{Ca}^{2+}$  in the STM channels.  $I$ - $V$  experiments involving the replacement of approximately symmetrical  $\text{Na}^+$  with an extracellular solution containing 50 mM  $\text{Ca}^{2+}$  and 57.5 mM  $\text{Na}^+$  resulted in a negative  $V_{\text{rev}}$  shift for the  $\text{Ca}^{2+}$ -containing solution ( $V_{\text{rev}} = -17.9 \pm 1.3$  mV ( $n = 4$ ), Fig. 5 D). This shift is equivalent to that expected from a dilution experiment, where  $[\text{Na}^+]_o$  has been reduced to 57.5 mM and where  $P_{\text{Ca}} \approx 0$ . This implied that  $\text{Ca}^{2+}$  has negligible permeability through the STM GlyR channels, in contrast to its permeability in the  $\alpha 7$  nAChR channels. The  $P_{\text{Ca}}/P_{\text{Na}}$  ratio was also calculated using Eq. 3 and found to be  $0.02 \pm 0.06$ , confirming a negligible  $\text{Ca}^{2+}$  permeability through the STM GlyRs.

### Single channel properties of WT and STM GlyRs

In three excised outside-out membrane patches from cells expressing WT GlyRs, bath application of 1 mM glycine induced inward currents ranging from  $\sim -200$  pA to  $-1$  nA, when the patches were clamped at a membrane potential of  $-60$  mV (e.g., Fig. 6, *inset*). In response to application of lower doses (1–100  $\mu\text{M}$ ) of glycine, single channel currents, often containing multiple conductance levels, were clearly discernible (Fig. 6). In close agreement with previous reports (Rajendra et al., 1995; Moorhouse et al., 1999), the dominant conductance level was  $\sim 93$  pS at  $-60$  mV. In these WT GlyR patches there was some inward rectification of this main conductance state, with the dominant peak in the all-point amplitude histogram for currents recorded at  $+60$  mV being 75 pS. Noise analysis, using measurements of variance, gave mean single channel conductances of  $74 \pm 6.2$  pS at  $-60$  mV ( $n = 3$ ) and  $49 \pm 14$  pS at  $+60$  mV ( $n =$

3). A reasonably similar ( $54 \pm 13$  pS) value of conductance in WT  $\alpha 1$ -homomeric GlyRs was recently reported by Saul et al. (1999) using non-stationary noise analysis. This lower value obtained with noise analysis should reflect contributions from each of the sub-conductance states. Indeed, in one of our patches that contained only two conductance states, weighting of the contribution of each of these states (directly measured) gave a similar value for the averaged conductance to that obtained using noise analysis (Fig. 6).

In contrast to the WT results, in excised patches containing STM GlyRs, clear glycine-activated currents were observed in only 4 of 7 patches clamped at  $-60$  mV and were much smaller, ranging from  $-2$  to  $-15$  pA in response to 100 mM glycine (Fig. 7). Even at lower doses we could not discern individual openings at  $-60$  mV. Noise analysis now gave very small average single channel conductance values:  $3.3 \pm 0.4$  pS at  $-60$  mV ( $n = 4$ ) and  $11.0 \pm 1.4$  pS at  $+60$  mV ( $n = 3$ ). This indicated that in contrast to anion currents in the WT GlyRs, there is a lower conductance for  $\text{Na}^+$  currents in the STM GlyRs, especially in the inward direction.

### Rectification of STM GlyRs

Whereas WT whole-cell and single channel currents showed some inward rectification (Figs. 2 and 6), STM GlyRs typically showed prominent outward rectification for both whole-cell and single channel currents (Figs. 3 and 5). For example, single channel rectification [defined as  $\gamma_{+60 \text{ mV}}/\gamma_{-60 \text{ mV}}$  for the weighted mean of all conductance levels], varied from  $\sim 0.7$  (inward) for WT GlyRs to  $\sim 3.3$  (outward) for STM GlyRs.

## DISCUSSION

Using the three equivalent inverse mutations, in the pore-forming M2 domain, that had been used to convert the  $\alpha 7$  nAChR channel from cationic to anionic (Galzi et al., 1992), we have been able to convert  $\alpha 1$  homomeric GlyRs from being predominantly anion-selective to being predominantly cation-selective. Thus, this study demonstrates that there is conservation of the molecular determinants of selectivity between the cationic and anionic LGICs. In addition to this fundamental change in ion selectivity, another key property conferred upon the STM GlyR was the monovalent permeability sequence ( $\text{Cs}^+ > \text{K}^+ > \text{Na}^+ > \text{Li}^+$ ), which is identical to that of the native nAChR (Adams et al., 1980; Quartararo et al., 1987; Konno et al., 1991; Villarreal and Sakmann, 1992). This suggests that the profile of the STM GlyR pore constriction region resembles that of the native nAChR. This is a low-field-strength permeation sequence, as is the permeation sequence for halide anions in native GlyRs (e.g., Bormann et al., 1987; Fatima-Shad and Barry, 1993). Other permeation properties of the STM GlyRs, namely the lack of  $\text{Ca}^{2+}$  permeability and the very

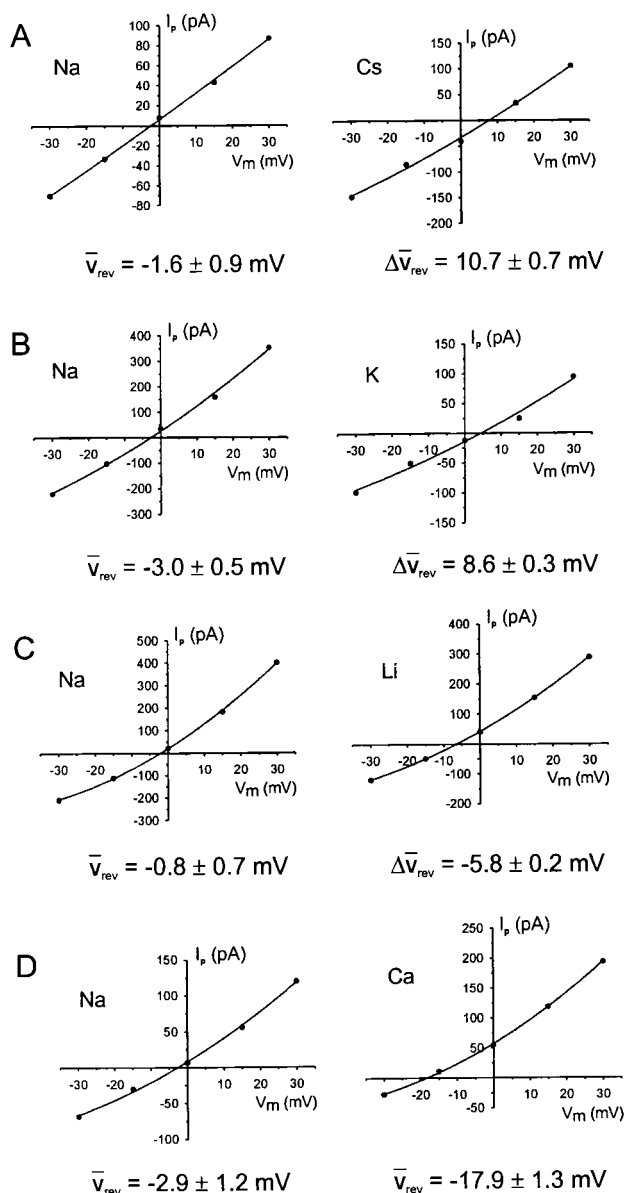


FIGURE 5 Examples of bi-ionic potential experiments for determining cation-selectivity sequences through the STM  $\alpha 1$  homomeric GlyR channels. Representative  $I$ - $V$  plots for a membrane potential range of  $-30$  mV to  $+30$  mV were fitted to a quadratic polynomial. Each panel represents a pair of  $I$ - $V$  plots measured for the same cell. In each case, the plot on the left represents data obtained in approximately symmetrical  $\text{Na}^+$  solutions and the plot on the right, data obtained after the replacement of the extracellular  $\text{Na}^+$  with the test cation shown. For the  $\text{Cs}^+$  experiments ( $n = 5$ ),  $[\text{Na}^+]_i = 160$  mM in both cases,  $[\text{Na}^+]_o = 149.3$  mM ( $\sim$ symmetrical  $\text{Na}^+$  case), and  $[\text{Cs}^+]_o = 149.3$  mM ( $\text{Cs}^+$  test case); for the  $\text{K}^+$  experiments ( $n = 4$ ),  $[\text{Na}^+]_i = 164.5$  mM in both cases,  $[\text{Na}^+]_o = 150$  mM ( $\sim$ symmetrical  $\text{Na}^+$  case), and  $[\text{K}^+]_o = 151.8$  mM ( $\text{K}^+$  test case); for the  $\text{Li}^+$  experiments ( $n = 4$ ),  $[\text{Na}^+]_i = 154.4$  mM in both cases,  $[\text{Na}^+]_o = 149.4$  mM ( $\sim$ symmetrical  $\text{Na}^+$  case),  $[\text{Li}^+]_o = 145$  mM and  $[\text{Na}^+]_o = 3.7$  mM ( $\text{Li}^+$  test case); and for the  $\text{Ca}^{2+}$  experiments ( $n = 4$ )  $[\text{Na}^+]_i = 164.5$  mM in both cases,  $[\text{Na}^+]_o = 150$  mM ( $\sim$ symmetrical  $\text{Na}^+$  case),  $[\text{Ca}^{2+}]_o = 50$  mM, and  $[\text{Na}^+]_o = 57.5$  mM ( $\text{Ca}^{2+}$  test case). Values, obtained by averaging the number of experiments done for each respective  $\bar{V}_{\text{rev}}$ , are quoted as mean  $\pm$  SEM. These shifts in reversal potential implied that  $P_{\text{Cs}} > P_{\text{K}} > P_{\text{Na}} > P_{\text{Li}} \gg P_{\text{Ca}} \approx 0$ .

low single channel conductance, are quite distinct from the homologous  $\alpha 7$  nAChR. The  $\text{Ca}^{2+}$  impermeability suggests that the STM GlyR has retained critical elements of the WT GlyR. In terms of the changes in properties brought about by both sets of mutations, there were similarities in that both caused alterations in current rectification and marked reductions in whole-cell currents (Galzi et al., 1992; Corringer et al., 1999). There were also radical differences in  $\text{EC}_{50}$ , in that comparatively high agonist concentrations were required to elicit currents in the STM GlyR, whereas a reduced  $\text{EC}_{50}$  was seen in the anionic nAChR triple mutant (Galzi et al., 1992).

The work presented in this study, together with the earlier mutagenesis work done by Galzi et al. (1992) identifying the anion-selective  $\alpha 7$  nAChRs triple mutant, provide evidence that at least two members of the LGIC superfamily, the anion-selective GlyR and the cation-selective nAChR, diverge in relatively minor ways with respect to the M2 pore-forming domains. These key differences impart not only profound properties regarding charge selectivity of the channels, but also other mechanistic properties essential for the physiological function of LGICs.

#### Pore constriction and possible physical mechanisms responsible for the conversion of charge selectivity in STM $\alpha 1$ subunit GlyRs

Ample experimental evidence now exists that the channel pore is narrowest at its intracellular end, in the region of the putative intermediate ring of charge found in all members of the LGIC family. Mutations to this ring in *Torpedo* nAChR have the most profound effect on channel conductance and monovalent cation selectivity in comparison with mutations in the extra- and intra-cellular rings (Imoto et al., 1988; Konno et al., 1991). These changes in conductance were inversely related to the size of the substituted residue, with a greater effect for hydrophobic than for polar substitutions (Imoto et al., 1991). The size and charge of residues of the intermediate ring have also been found to be determinants of permeability for organic cations (Wang and Imoto, 1992), indicating that both steric and electrostatic factors affect permeation in this region. This position, corresponding to A251 (A-1') in the primary sequence of  $\alpha 1$  GlyRs, is functionally more analogous to the GlyR charged ring at R252 (R0').

In addition to this intermediate charged ring, an adjacent ring of polar amino acids is also a major determinant of monovalent cation permeation, in both rat and *Torpedo* nAChR (corresponding to G254 (G2') in  $\alpha$  GlyRs). Mutagenesis studies of this polar ring in the rat nAChR (Villarroel et al., 1992; Villarroel and Sakmann, 1992) and *Torpedo* AChRs (Imoto et al., 1991) have suggested that in this region cation permeation is sterically regulated. More recently, the SCAM technique has demonstrated that residues in this region present a barrier to large methanethio-

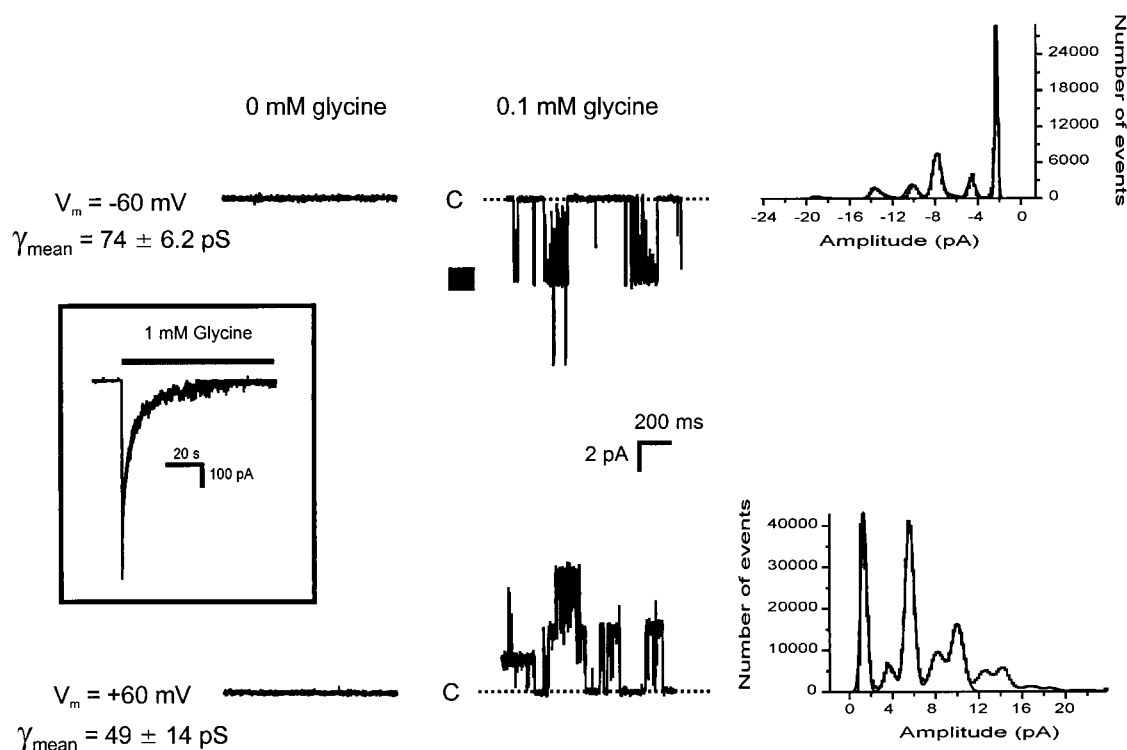


FIGURE 6 Single channel activity in WT homomeric  $\alpha 1$  GlyRs. Single channel currents obtained from an outside-out membrane patch expressing WT  $\alpha 1$  homomeric GlyRs at membrane potentials of  $-60$  mV (*above*) and  $+60$  mV (*below*). The averaged mean conductance ( $\gamma_{\text{mean}}$ ), obtained from noise analysis is shown for membrane potentials of  $-60$  mV ( $n = 3$  patches) and  $+60$  mV ( $n = 3$  patches). The main peak conductance obtained by fitting Gaussian distributions to all-point histograms and confirmed by direct measurement is  $\sim 93$  pS at  $-60$  mV and  $\sim 75$  pS at  $+60$  mV. The right panels show all-point current histograms from 30 to 50 s of continuous data, fitted with multiple (5) Gaussian distributions between 0 and  $-16$  pA (*top panel*;  $-60$  mV) and between 0 and 12 pA (*bottom panel*;  $+60$  mV) with bin size 0.20 pA. The first peak (closest to 0) on the histograms represents the current baseline. Note also evidence of inward rectification, with inward currents being greater than outward currents (ratio  $\approx 1.5$ ). The inset shows a macropatch response to 1 mM glycine recorded from the same patch. For display, data were filtered off-line with a further 1 kHz digital, Gaussian filter and also reduced by a factor of 4.

sulfonate cations from both the extra- and intra-cellular sides (Wilson and Karlin, 1998; Pascual and Karlin, 1998). The results indicated that, in the absence of agonist, residues between 2' and  $-3'$  presented a barrier to the reagents but, in the presence of agonist, this barrier was partially removed. This suggested that there are structural perturbations within the pore constriction region during the gating process of the channel. By analogy, these AChR residues correspond to those between A249 (A-3') and G245 (G2') in the  $\alpha 1$  GlyR (Fig. 1). In the closely homologous GABA<sub>A</sub>R, the SCAM method has also been used to experimentally ascertain the location of the charge selectivity filter and the region that acts as a barrier to methanethio-sulfonate anions (Xu et al., 1995; Xu and Akabas, 1996). Those results showed that the selectivity filter was more cytoplasmic than the  $\alpha 1$  GABA<sub>A</sub>R residue T6' (T258 in  $\alpha 1$  GlyR), while the most constricted region of the GABA<sub>A</sub>R pore was even more cytoplasmic than residue V2' (G254 in the  $\alpha 1$  GlyR). Similarly, Tierney et al. (1998) have shown that mutations to polar threonine residues in the GABA<sub>A</sub>R (T6') can block anion permeation, while Bormann et al.

(1993) determined that the  $\alpha 1$  homomeric GlyR mutant, G254A (G2'A), caused an increase in single channel conductance levels. Together, these results indicate that in this extended region there are residues which, due to their polarity and size, provide an environment that is most ideally suited for partially hydrated ions of a particular size.

Our results more definitively indicate that the  $\alpha 1$  GlyR STM presented in this study resembles that of the WT  $\alpha 7$  nAChR with regard to the putative narrow pore constriction region, and that the most selective part of the channel, at least with regard to monovalent ions, lies within that region. We propose that the deletion of a proline (P250 $\Delta$ ; P-2' $\Delta$ ) and the A251E (A-1'E) substitution have made fundamental alterations to the geometrical and electrostatic environment of the pore constriction region, presumably allowing the glutamate to face the pore interior and aid in the selection of cations, and causing the adjacent arginine (R252; R0') to be moved away from the pore interior and less able to repel cations (cf. K0' in the  $\alpha 7$  nAChR; see Fig. 1). This inference is supported by recent evidence suggesting that the K0' residue in the mouse AChR does not interact directly with

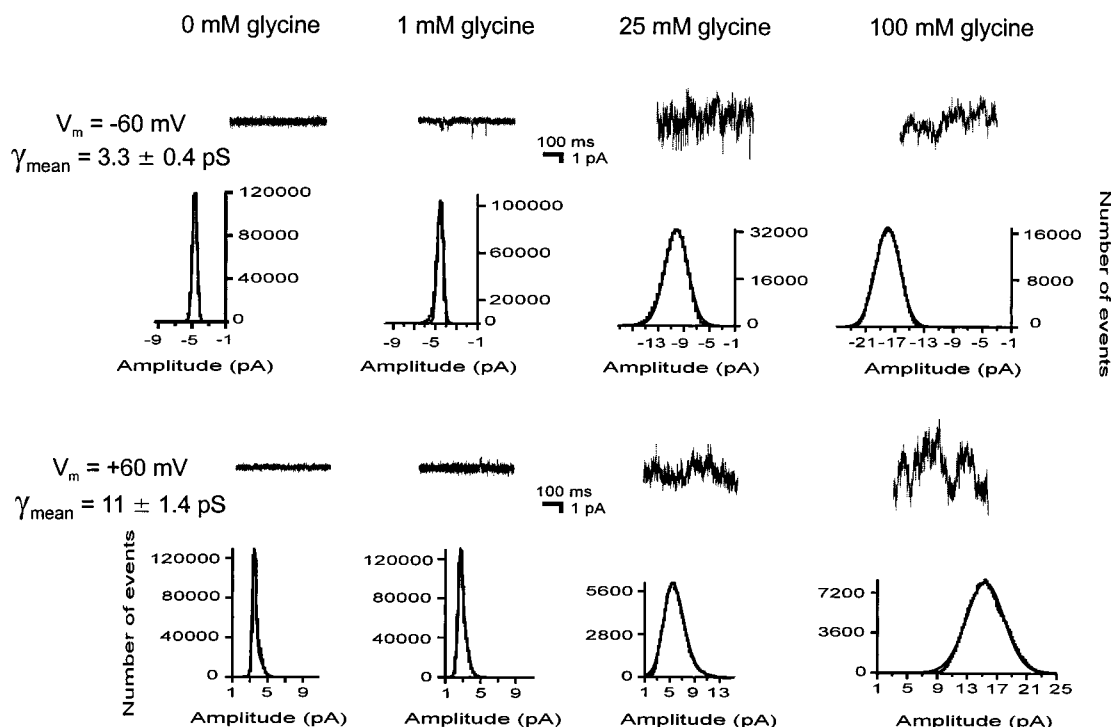


FIGURE 7 Single channel activity in STM homomeric  $\alpha 1$  GlyRs. Single channel currents obtained from an outside-out membrane patch expressing STM  $\alpha 1$  homomeric GlyRs at membrane potentials of  $-60$  mV (*top panels*) and  $+60$  mV (*bottom panels*). The averaged mean conductance ( $\gamma_{\text{mean}}$ ) obtained from noise analysis is shown for membrane potentials of  $-60$  mV ( $n = 4$  patches) and  $+60$  mV ( $n = 3$  patches). Below each channel recording are the corresponding all-point current histograms from 30–60s of continuous data, which showed a graded increase in current amplitude as the glycine concentration was increased. For display, data were filtered off-line with a further 1 kHz digital, Gaussian filter and also reduced by a factor of 4. All-point histograms were fitted with a single (or sometimes 2) Gaussian distribution(s) with bin size 0.09–0.19 pA.

permeating ions (Wilson et al., 2000). The obvious mutation, which would seem to combine the proposed functions of the two intracellular mutations P250 $\Delta$  (P-2') and A251E (A-1'), would be the direct mutation of the positive arginines (R252; R0') to a negative glutamate or aspartate. However, previous experiments to mutate this residue to a more conservative asparagine residue (R252N; R0'N) did not appear to elicit any currents, and failed to demonstrate any strychnine binding (Rajendra, 1995). Also, antibody experiments by Langosch et al. (1993), in which they had mutated this residue to either glutamine (R252Q; R0'Q) or glutamate (R252E; R0'E), seemed to indicate that these residues prevented GlyR expression on the cell surface. Thus, R252 (R0') may also play a critical structural role in the WT GlyR. However, in the AChR, mutations of the equivalent residue (K0') to cysteine are tolerated and it appears to move during channel gating (Wilson and Karlin, 1998; Wilson et al., 2000). We would suggest that for our STM GlyRs both the P250 $\Delta$  (P-2' $\Delta$ ) and A251E (A-1'E) mutations are responsible for monovalent selectivity conversion, and that the T265V (T13'V) may not even be required. The need for both cytoplasmic mutations is supported by the recent evidence that the proline residue, P250

(P-2') in the  $\alpha 1$  GlyRs, when genetically disrupted as P250T (P-2'T) by hereditary hyperekplexia, markedly impairs single channel  $\text{Cl}^-$  conductance, but is not sufficient to change the charge selectivity (Saul et al., 1999).

In summary, we propose that both a negative charge introduction A251E (A-1'E) and a conformational change to displace the positively charged residue (R252; R0'), caused primarily by the P250 $\Delta$  (P-2' $\Delta$ ) in this constricted region is required to convert charge selectivity in the GlyR.

### Effects of the STM mutations on channel gating

In addition to the fundamental change in ion selectivity discussed above, the STM GlyR also showed some distinct changes in the gating behavior of the channel. This included a marked increase in the agonist concentration required to open the channel (with an implied large increase in  $\text{EC}_{50}$ ) and a large decrease in maximum current amplitude. These effects are characteristic of a "loss of function" mutation and are the opposite to the "gain of function" characteristics observed in the nAChR selectivity triple mutant, attributed largely to the "permissive" V13'T mutation (Galzi et al.,

1992; Corringer et al., 1999). Consequently, we infer that the effects of a threonine-valine mutation at the corresponding position in the GlyR has a similar effect on the open-closed equilibrium of the channel, but in the case of the STM GlyR conversion of a threonine to a valine would impair the gating of the open or active state. Thus, it is not surprising that, in contrast to Corringer et al. (1999), no spontaneous openings were observed in STM GlyR channels (as judged by the lack of baseline fluctuations in control conditions in the single channel recordings and by the lack of any differences in the mean holding current in the whole-cell recordings, data not shown), since the closed-to-open transitions would be more difficult, and hence spontaneous openings would be less likely. Indeed, the T265V (T13'V) mutation may not be necessary to produce a GlyR cation-selective channel, and may even be counterproductive to channel activation.

The reduced rate of current decay in the STM in comparison with WT GlyRs may reflect the very much smaller currents of the STM GlyRs and a lack of local concentration polarization effects, which would be more substantial with large WT currents, rather than due to a change in GlyR desensitization.

### Reduced single channel conductance and altered rectification in STM $\alpha 1$ subunit GlyRs

It is well established that the charged rings flanking the pore region of LGICs influence conductance and channel gating. With regard to conductance and the charged extracellular ring, Imoto et al. (1988) have shown that the conductance decreased linearly with a reduction in the total negative charge of the ring. Mutagenesis experiments on anionic  $\alpha 1$  homomeric GlyRs have also shown that when the positively charged ring, R271 (R19'), is mutated to a neutral glutamine, R271Q (R19'Q), or to a neutral leucine, R271L (R19'L), changing its charge from +5 to 0, the GlyR conductance decreased similarly to ~20% of WT values (Langosch et al., 1994; Rajendra et al., 1995), which is approximately the equivalent proportional change predicted from the data of Imoto et al. (1988) for the AChR. Importantly, no change in channel selectivity was observed in these mutants (Konno et al., 1991; Rajendra et al., 1994, 1995).

Partial neutralization of the extracellular ring as seen in  $\alpha 1/\beta$  heteromeric GlyRs has also been reported to display lower conductance than in the  $\alpha 1$  homomeric channels (Bormann et al., 1993). Similarly, in the GABA<sub>A</sub>R homolog, the *Rdl* gene product, introducing a negatively charged aspartate to this position, N19'D, produced a fall in channel conductance, while the N19'R and N19'K mutants both showed an increase in channel conductance (Wang et al., 1999). We would suggest that the charge lining the extracellular vestibule of the pore helps to determine the concentration of oppositely charged ions near the pore con-

striction (see Dani, 1986), and in this way contributes to the magnitude of the single channel conductance. It therefore seems reasonable to infer that if the effect of the STM proline deletion, P250 $\Delta$  (P-2' $\Delta$ ), has not caused enough of a structural change along the whole M2 region to significantly move the R271 (R19') from a position lining the channel interior, the positively charged ring would remain exposed for the permeating ions. This means that the STM GlyR will now have an inappropriate +5 charge (instead of the -5 charge in the  $\alpha 7$  nAChR) lining the channel pore for a cationic channel. This charge may then substantially lower the concentration of cations in this vestibule region and hence radically decrease the conductance of the channel, as observed in our outside-out patches (Fig. 7) and result in very small whole-cell currents (Fig. 3). In addition, the relatively low cation concentration at the extracellular end of the STM GlyR pore would also explain the outward rectification noted for both single channel and whole-cell currents in the mutant receptors, since inward current should be especially reduced. This circumstance is equivalent to that seen in the *Torpedo* AChR by Imoto et al. (1988), where the  $\alpha E19'K$  AChR mutant produced low conductance values and an outwardly rectifying current. The  $\alpha 7$  nAChR anionic mutations investigated by Galzi et al. (1992) and Corringer et al. (1999) showed a weaker alteration of rectification, with the triple mutant anionic channel displaying no rectification compared to the inwardly rectifying WT channels. The STM GlyR rectification behavior is consistent with an asymmetry of charges lining the channel pore and supports two of our conclusions for the STM GlyR: namely, that the internal charged R252 (R0') has been shielded or at least moved away from the pore interior, and that there are only local structural changes along the M2 region, so that the position of the external R271 (R19') is relatively unaltered.

### Lack of Ca<sup>2+</sup> permeability in STM $\alpha 1$ subunit GlyRs

Previous studies have shown that the  $\alpha 7$  nAChR has a significant Ca<sup>2+</sup> permeability ( $P_{Ca}/P_{Na} \sim 10$ ; Bertrand et al., 1993). A substantial difference between the AChR and the STM GlyR is that the latter displayed an inability to conduct Ca<sup>2+</sup> ions in either direction (Fig. 5 D). The mutation of the  $\alpha 7$  nAChR intermediate ring glutamate (E-1'A) makes this channel impermeable to Ca<sup>2+</sup>. The reverse mutation is not sufficient to restore it. This is not surprising, since many other nAChR mutations also reduce its calcium permeability. We, therefore, propose that other residues must confer a difference in pore geometry between the STM GlyR and the WT  $\alpha 7$  nAChR. For example, adjacent leucines (L16' and L17') found in the  $\alpha 7$  nAChR, when mutated, are reported to drastically reduce Ca<sup>2+</sup> permeability without effecting monovalent cation permeability (Bertrand et al., 1993). In the  $\alpha 1$  GlyR the equivalent positions

are occupied by serine S268 (S16') and glycine G269 (G17'). The absence of the leucines from the STM channels may play a significant role in excluding  $\text{Ca}^{2+}$  ions from entering the pore. Furthermore, the positively charged arginines (R271; R19') at the extracellular mouth of the GlyR are also likely to prevent  $\text{Ca}^{2+}$  transport through the STM GlyR by radically reducing its concentration in that region. In addition, the STM channels carry the T265V (T13'V) substitution, which would also be expected to attenuate  $\text{Ca}^{2+}$  permeability (Bertrand et al., 1993). Thus, it is not surprising that the STM GlyR is impermeable to  $\text{Ca}^{2+}$  ions. We speculate that mutating the R271 (R19') to a negatively charged residue and restoring the T265 (T13') threonine residue in the GlyR, if it still allows functional channels, may help to provide a localized pore conformation more favorable to  $\text{Ca}^{2+}$  ions.

## CONCLUSIONS

Three mutations in the M2 transmembrane domains of the anion-selective GlyR have successfully converted it to a cation-selective channel with a low-field-strength cation permeability sequence, an impermeability to  $\text{Ca}^{2+}$ , and a low single channel conductance.

We thank Kerrie Pierce for constructing the mutants, and Anna Scimone and Irene Michas for preparing the cell transfections. Discussions with Drs. Nishith Mahanti and Sundran Rajendra were much appreciated. We also thank Dr. Trevor Lewis for critical reading of the manuscript.

This work was supported by the National Health and Medical Research Council of Australia and the Australian Research Council.

## REFERENCES

- Adams, D. J., T. M. Dwyer, and B. Hille. 1980. The permeability of endplate channels to monovalent and divalent metal cations. *J. Gen. Physiol.* 75:493–510.
- Barry, P. H. 1994. JPCalc, a software package for calculating liquid junction potential corrections in patch-clamp, intracellular, epithelial and bilayer measurements and for correcting junction potential measurements. *J. Neurosci. Meth.* 51:107–116.
- Barry, P. H., and P. W. Gage. 1984. Ion selectivity of channels at the end-plate. In *Current Topics in Membranes and Transport*. W. D. Stein, editor. Academic Press, London. 21:1–51.
- Barry, P. H., and J. W. Lynch. 1991. Liquid junction potentials and small cell effects in patch-clamp analysis. *J. Membr. Biol.* 121:101–107.
- Bertrand, D., J. L. Galzi, A. Devillers-Thiéry, S. Bertrand, and J. P. Changeux. 1993. Mutations at two distinct sites within the channel domain M2 alter calcium permeability of neuronal  $\alpha 7$  nicotinic receptor. *Proc. Natl. Acad. Sci. USA.* 90:6971–6975.
- Bormann, J., O. P. Hamill, and B. Sakmann. 1987. Mechanism of anion permeation through channels gated by glycine and GABA in mouse cultured spinal neurons. *J. Physiol. (Lond.)* 385:243–286.
- Bormann, J., N. Rundstrom, H. Betz, and D. Langosch. 1993. Residues within transmembrane segment M2 determine chloride conductance of glycine receptor homo- and hetero-oligomers. *EMBO J.* 12:3729–3737.
- Chen, C., and H. Okayama. 1987. High efficiency expression of mammalian cells by plasmid DNA. *Mol. Cell. Biol.* 7:2745–2751.
- Corringer, P. J., S. Bertrand, J. L. Galzi, A. Devillers-Thiéry, J. P. Changeux, and D. Bertrand. 1999. Mutational analysis of the charge selectivity filter of the  $\alpha 7$  nicotinic acetylcholine receptor. *Neuron.* 22: 831–843.
- Dani, J. A. 1986. Ion-channel entrances influence permeation. *Biophys. J.* 49:607–618.
- Eisenman, G., and R. Horn. 1983. Ionic selectivity revisited: the role of kinetic and equilibrium processes in ion permeation through channels. *J. Membr. Biol.* 76:197–225.
- Fatima-Shad, K., and P. H. Barry. 1993. Anion permeation in GABA- and glycine-gated channels of mammalian hippocampal neurons. *Proc. R. Soc. Lond. B.* 253:69–75.
- Galzi, J. L., A. Devillers-Thiéry, N. Hussey, S. Bertrand, J. P. Changeux, and D. Bertrand. 1992. Mutations in the channel domain of a neuronal nicotinic receptor convert ion selectivity from cationic to anionic. *Nature.* 359:500–505.
- Gray, P. T. A. 1994. Analysis of whole cell currents to estimate the kinetics and amplitude of unitary events: relaxation and 'noise' analysis. In *Microelectrode Techniques*, 2nd Ed. D. Ogden, editor. The Company of Biologists Limited, Cambridge. 189–207.
- Imoto, K., C. Busch, B. Sakmann, M. Mishina, T. Konno, J. Nakai, H. Bujo, Y. Mori, K. Fukuda, and S. Numa. 1988. Rings of negatively charged amino acids determine the acetylcholine receptor channel conductance. *Nature.* 335:645–648.
- Imoto, K., T. Konno, J. Nakai, F. Wang, M. Mishina, and S. Numa. 1991. A ring of uncharged polar amino acids as a component of channel constriction in the nicotinic acetylcholine receptor. *FEBS Lett.* 289: 193–200.
- Karlin, A., and M. H. Akabas. 1995. Toward a structural basis for the function of nicotinic acetylcholine receptors and their cousins. *Neuron.* 15:1231–1244.
- Konno, T., C. Busch, E. Von Kitzing, K. Imoto, F. Wang, J. Nakai, M. Mishina, S. Numa, and B. Sakmann. 1991. Rings of anionic amino acids as structural determinants of ion selectivity in the acetylcholine receptor channel. *Proc. R. Soc. Lond. B.* 244:69–79.
- Kuhse, J., H. Betz, and J. Kirsch. 1995. The inhibitory glycine receptor: architecture, synaptic localization and molecular pathology of a postsynaptic ion-channel complex. *Curr. Opin. Neurobiol.* 5:318–323.
- Langosch, D., A. Herbold, V. Schmieden, J. Bormann, and J. Kirsch. 1993. Importance of Arg-219 for correct biogenesis of  $\alpha 1$  homooligomeric glycine receptors. *FEBS Lett.* 336:540–544.
- Langosch, D., B. Laube, N. Rundstrom, V. Schmieden, J. Bormann, and H. Betz. 1994. Decreased agonist affinity and chloride conductance of mutant glycine receptors associated with human hereditary hyperekplexia. *EMBO J.* 13:4223–4228.
- Langosch, D., L. Thomas, and H. Betz. 1988. Conserved quaternary structure of ligand-gated ion channels: the post synaptic glycine receptor is a pentamer. *Proc. Natl. Acad. Sci. USA.* 85:7394–7398.
- Lynch, J. W., S. Rajendra, K. D. Pierce, C. A. Handford, P. H. Barry, and P. R. Schofield. 1997. Identification of intracellular and extracellular domains mediating signal transduction in the inhibitory glycine receptor chloride channel. *EMBO J.* 16:110–120.
- Miller, C. 1989. Genetic manipulation of ion channels: a new approach to structure and mechanism. *Neuron.* 2:1195–1205.
- Moorhouse, A. J., P. Jacques, P. H. Barry, and P. R. Schofield. 1999. The startle disease mutation Q266H, in the second transmembrane domain of the human glycine receptor, impairs gating. *Mol. Pharmacol.* 55: 386–395.
- Pascual, J. M., and A. Karlin. 1998. State-dependent accessibility and electrostatic potential in the channel of the acetylcholine receptor. *J. Gen. Physiol.* 111:171–179.
- Quartararo, N., P. H. Barry, and P. W. Gage. 1987. Ion permeation through single channels activated by acetylcholine in denervated toad sartorius muscle fibers: effects of alkali cations. *J. Membr. Biol.* 97:137–159.
- Rajendra, S. 1995. Molecular determinants of ligand binding and channel activation in the human glycine receptor. Ph.D. Thesis, The University of New South Wales, Sydney, Australia.
- Rajendra, S., J. W. Lynch, K. D. Pierce, C. R. French, P. H. Barry, and P. R. Schofield. 1994. Startle disease mutations reduce the agonist

- sensitivity of the human inhibitory glycine receptor. *J. Biol. Chem.* 269:18739–18742.
- Rajendra, S., J. W. Lynch, K. D. Pierce, C. R. French, P. H. Barry, and P. R. Schofield. 1995. Mutation of an arginine residue in the human glycine receptor transforms  $\beta$ -alanine and taurine from agonists to competitive antagonists. *Neuron*. 14:169–175.
- Robinson, R. A., and R. H. Stokes, 1965. *Electrolyte Solutions*, 2nd Ed., revised. Butterworths, London.
- Sansom, M. S. P. 1995. Twist to open. *Curr. Biol.* 5:373–375.
- Saul, B., T. Kuner, D. Sobetzko, W. Brune, F. Hanefeld, H. M. Meinck, and C. M. Becker. 1999. Novel GLRA1 missense mutation (P250T) in dominant hyperekplexia defines an intracellular determinant of glycine receptor channel gating. *J. Neurosci.* 19:869–877.
- Tierney, M. L., B. Birnir, B. Cromer, S. M. Howitt, P. W. Gage, and G. B. Cox. 1998. Two threonine residues in the M2 segment of the  $\alpha_1\beta_1$  GABA<sub>A</sub> receptor are critical for ion channel function. *Receptors and Channels*. 5:113–124.
- Unwin, N. 1995. The acetylcholine receptor channel imaged in the open state. *Nature*. 373:37–43.
- Villarroel, A., S. Herlitze, V. Witzemann, M. Koenen, and B. Sakmann. 1992. Asymmetry of the rat acetylcholine receptor subunits in the narrow region of the pore. *Proc. R. Soc. Lond. B.* 249:317–324.
- Villarroel, A., and B. Sakmann. 1992. Threonine in the selectivity filter of the acetylcholine receptor channel. *Biophys. J.* 62:196–208.
- Wang, F., and K. Imoto. 1992. Pore size and negative charge as structural determinants of permeability in the *Torpedo* nicotinic acetylcholine receptor channel. *Proc. R. Soc. Lond. B.* 250:11–17.
- Wang, C. T., H. G. Zhang, T. A. Rocheleau, R. H. French-Constant, and M. B. Jackson. 1999. Cation permeability and cation-anion interactions in a mutant GABA-gated chloride channel from *Drosophila*. *Biophys. J.* 77:691–700.
- Wilson, G. G., and A. Karlin. 1998. The location of the gate in the acetylcholine receptor channel. *Neuron*. 20:1269–1281.
- Wilson, G. G., P. M. Pascual, N. Brooijmans, D. Murray, and A. Karlin. 2000. The intrinsic electrostatic potential and the intermediate ring of charge in the acetylcholine receptor channel. *J. Gen. Physiol.* 115: 93–106.
- Xu, M., and M. H. Akabas. 1996. Identification of channel-lining residues in the M2 membrane-spanning segment of the GABA<sub>A</sub> receptor  $\alpha_1$  subunit. *J. Gen. Physiol.* 107:195–205.
- Xu, M., D. F. Covey, and M. H. Akabas. 1995. Interaction of picrotoxin with GABA<sub>A</sub> receptor channel-lining residues probed in cysteine mutants. *Biophys. J.* 69:1858–1867.